Water Vapor in the Protoplanetary Disk of DG Tau

Podio, L.; Kamp, I.; Codella, C.; Cabrit, S.; Nisini, B.; Dougados, C.; Sandell, G.; Williams, J. P.; Testi, L.; Thi, W. -F.

Published in:
Astrophysical Journal Letters

DOI:
10.1088/2041-8205/766/1/L5

Publication date:
2013

The Astrophysical Journal Letters, 766:L5 (5pp), 2013 March 20 doi:10.1088/2041-8205/766/1/L5

WATER VAPOR IN THE PROTOPLANETARY DISK OF DG Tau

L. Podio[1], I. Kamp[2], C. Codella[3], S. Cabrit[4], B. Nisini[5], C. Dougados[1,6], G. Sandell[7], J. P. Williams[8], L. Testi[9], W.-F. Thi[1], P. Woitke[10], R. Meijerink[2], M. Spaans[2], G. Aresu[2], F. Ménard[1,6], and C. Pinte[1]
[1] UJF-Grenoble 1/CNRS-INSU, Institut de Planétologie et d'Astrophysique de Grenoble (IPAG) UMR 5274, F-38041 Grenoble, France
[2] Kapteyn Astronomical Institute, University of Groningen, Landleven 12, 9747 AD Groningen, The Netherlands
[3] INAF-Osservatorio Astrofisico di Arcetri, Largo E. Fermi 5, I-50125 Florence, Italy
[4] LERMA, UMR 8112 du CNRS, Observatoire de Paris, École Normale Supérieure, Université Pierre et Marie Curie, Université de Cergy-Pontoise, 61 Av. de l'Observatoire, F-75014 Paris, France
[5] INAF-Osservatorio Astronomico di Roma, via di Frascati 33, I-00040 Monte Porzio Catone, Italy
[6] LFCA, UMI 3386, CNRS and Departamento de Astronomia, Universidad de Chile, Santiago, Chile
[7] SOFIA-USRA, NASA Ames Research Center, MS 232-12, Building N232, Rm. 146, P.O. Box 1, Moffett Field, CA 94035-0001, USA
[8] Institute for Astronomy (IfA), University of Hawaii, 2680 Woodlawn Dr., Honolulu, HI 96822, USA
[9] European Southern Observatory, Karl-Schwarzschild-Strasse 2, D-85748 Garching, Germany
[10] SUPA, School of Physics and Astronomy, University of St. Andrews, KY16 9SS, UK
Received 2013 January 19; accepted 2013 February 5; published 2013 March 1

ABSTRACT

Water is key in the evolution of protoplanetary disks and the formation of comets and icy/water planets. While high-excitation water lines originating in the hot inner disk have been detected in several T Tauri stars (TTSs), water vapor from the outer disk, where most water ice reservoirs are stored, was only reported in the nearby TTS TW Hya. We present spectrally resolved *Herschel*/HIFI observations of the young TTS DG Tau in the ortho- and para-water ground-state transitions at 557 and 1113 GHz. The lines show a narrow double-peaked profile, consistent with an origin in the outer disk, and are ∼19–26 times brighter than in TW Hya. In contrast, CO and [C II] lines are dominated by emission from the envelope/outflow, which makes H_2O lines a unique tracer of the disk of DG Tau. Disk modeling with the thermo-chemical code ProDiMo indicates that the strong UV field, due to the young age and strong accretion of DG Tau, irradiates a disk upper layer at 10–90 AU from the star, heating it up to temperatures of 600 K and producing the observed bright water lines. The models suggest a disk mass of 0.015–0.1 $M_\odot$, consistent with the estimated minimum mass of the solar nebula before planet formation, and a water reservoir of $\sim 10^2$–10^3 Earth oceans in vapor and ∼100 times larger in the form of ice. Hence, this detection supports the scenario of ocean delivery on terrestrial planets by the impact of icy bodies forming in the outer disk.

Key words: astrochemistry – ISM: molecules – protoplanetary disks – stars: individual (DG Tau)

Online-only material: color figures

1. INTRODUCTION

Protoplanetary disks are the birthplaces of planets; thus, the study of their physical and chemical structure is fundamental to comprehending the formation of our own solar system as well as that of extrasolar planetary systems. One of the most intriguing issues related to planet formation concerns the origin of the Earth's oceans. It was argued that Earth formed as a dry planet and that ocean water was delivered by impacts of icy bodies/protocomets originating from the cold outer disk, where most of the mass (and water reservoir) is located (Matsui & Abe 1986). To address this issue, several efforts have been devoted to observing water in protoplanetary disks and to characterizing its abundance and spatial distribution.

In the hot dense inner disk region inside the so-called snow line where $T_{\rm dust} \sim 150$ K, i.e., for radii smaller than ∼1–3 AU in disks around T Tauri Stars (TTSs; Lecar et al. 2006), ice cannot exist on dust grains and gas-phase chemistry converts all oxygen into water on timescales short compared to the disk evolution timescale. Beyond the snow line, instead, water molecules will be frozen onto dust grains. However, (inter)stellar UV and X-ray radiation can penetrate the disk upper layers and photodesorb a fraction of water ice back into the gas phase (Ceccarelli et al. 2005; Dominik et al. 2005). The released water vapor may be eventually dissociated and re-formed in the gas phase.

H_2O lines with upper level energies $E_{\rm up} > 1000$ K, tracing hot water vapor in the inner disk regions, have now been observed in a number of protoplanetary disks thanks to ground-based and *Spitzer* near- and mid-infrared observations (e.g., Carr & Najita 2008; Salyk et al. 2008; Pontoppidan et al. 2010a, 2010b), and, recently, far-infrared observations of the 63.32 μm line with *Herschel* (Riviere-Marichalar et al. 2012). In contrast, cold water vapor at $T < 200$ K from the outer disk surface has been revealed to be surprisingly difficult to detect in TTSs. *Herschel*/PACS detected the low-excitation H_2O 179.5 μm line ($E_{\rm up} = 114$ K) only in jet-driving stars, but due to the lack of spatial and velocity information, it is unclear if it originates in the disk or in the envelope/outflow (Podio et al. 2012). Until now, firm evidence for a cold disk water reservoir has been found only in the nearby ($d \sim 50$ pc) TTS TW Hya, through the detection of the fundamental ortho and para lines at 557 and 1113 GHz with the *Herschel*/Heterodyne Instrument for the Far Infrared (HIFI; Hogerheijde et al. 2011). While o-H_2O 557 GHz line profiles in Class 0 and I sources show velocities of ∼11–138 km s^{-1} and ∼5–54 km s^{-1}, suggesting that they are dominated by emission from the envelope/outflow (Kristensen et al. 2012), the H_2O emission from TW Hya shows a narrow single-peaked profile (FWHM ∼ 0.96–1.2 km s^{-1}) consistent with an origin in the face-on disk. A hidden reservoir of icy bodies of 1.5 $M_\oplus$ equivalent to several thousands of Earth oceans[11] is inferred. Additional studies are necessary to investigate this hypothesis, but only upper limits were obtained toward a couple of other TTSs targeted with HIFI, e.g., DM Tau (Bergin et al. 2010).

[11] 1 $M_\oplus = 5.97 \times 10^{27}$ g and 1 Earth ocean $\simeq 1.5 \times 10^{24}$ g.

DG Tau is a young TTS at 140 pc associated with particularly strong accretion/outflow activity (e.g., Hartigan et al. 1995; Dougados et al. 2000), and where we previously detected unresolved emission in the H_2O 78.7, 179.5 μm lines with *Herschel*/PACS (Podio et al. 2012). In this Letter, we present clear detections of the H_2O 557, 1113 GHz lines toward this source.

2. OBSERVATIONS AND DATA REDUCTION

We observed DG Tau ($\alpha_{J2000} = 04^h27^m04^s.7$, $\delta_{J2000} = +26°06'16''.3$) with HIFI (de Graauw et al. 2010) on board the *Herschel Space Observatory*[12] (Pilbratt et al. 2010). The observations target the two fundamental water lines, o-H_2O 1_{10}-1_{01} and p-H_2O 1_{11}-0_{00}, the ^{12}CO (hereafter CO) and ^{13}CO 10–9, and the [C II]^2 $P_{3/2}$-$^2P_{1/2}$ lines (ObsIDs: 1342239630, 1342250208, 1342249594, 1342249646). They were acquired in HIFI bands 1, 4, 5, and 7, with a single on-source pointing and in dual-beam switch mode with fast chopping 3′ either side of the target. The Wide Band Spectrometer (WBS) and the High Resolution Spectrometer (HRS) were used in parallel, with a spectral resolution of 1.10 and 0.25 MHz, respectively. The half-power beam width (HPBW) ranges from ∼11″ to ∼38″, depending on frequency.

HIFI data were reduced using HIPE 8.[13] Fits files from level 2 were then created and transformed into the GILDAS[14] format for data analysis. The spectra were baseline subtracted and then resampled at 0.6 km s^{-1} to increase the sensitivity. Note that the V-spectrum of the o-H_2O and p-H_2O lines is affected by ripples, degrading the quality of the baseline and resulting in an rms larger than the one measured in the H-spectrum. Therefore, in the following, we will analyze the o-H_2O and p-H_2O emission based solely on the H-spectrum.

The HIFI data set is complemented by observations of the CO 3–2 line performed on 2010 January at the 15 m James Clerk Maxwell Telescope (JCMT; Mauna Kea, HI, USA) using the HARP-B heterodyne array and ASCIS correlator, providing a spectral resolution of 0.25 km s^{-1}. The spectrum was resampled at 0.6 km s^{-1} to be compared with the HIFI data.

Antenna temperatures, T_a, are converted to mean beam temperature, T_{mb} (HIFI mean beam efficiencies are from Roelfsema et al. 2012). Integrated line intensities, $\int T_{mb}dV$, and line fluxes, $F_{obs} = (2K_b\nu^3/c^3)\times\int T_{mb}dV\times\pi(\mathrm{HPBW}/2\sqrt{\ln 2})^2$, are summarized in Tables 1 and 3.

3. RESULTS FROM OBSERVATIONS

The observed line profiles are shown in Figure 1. The JCMT CO 3–2 line profile in panel (a) suggests that the systemic velocity is $V_{sys} \sim +6.2$ km s^{-1}, consistent with previous studies (Schuster et al. 1993; Kitamura et al. 1996; Testi et al. 2002).

We detect both the ortho-H_2O 1_{10}-1_{01} 557 GHz and the para-H_2O 1_{11}-0_{00} 1113 GHz lines ($E_{up} \sim 61$, 53 K) with a signal-to-noise ratio of 10 and 12, respectively. They are centered at the systemic velocity and show a narrow double-peaked profile (FWHM ∼ 5–6 km s^{-1}).

Table 1
Line-integrated Intensities

Transition[a]	ν_0[b] (GHz)	η_{mb}	HPBW (″)	$\int T_{mb}dV$ (K km s^{-1})
o-H_2O 1_{10}-1_{01}	556.936	0.76	38	0.10 ± 0.01
p-H_2O 1_{11}-0_{00}	1113.343	0.74	19	0.12 ± 0.01
CO 10–9	1151.985	0.64	18	5.8 ± 0.1
^{13}CO 10–9	1101.350	0.74	19	0.28 ± 0.01
[C II] $^2P_{3/2}$-$^2P_{1/2}$	1900.537	0.69	11	3.1 ± 0.2
CO 3–2	345.795	0.66	14	32.5 ± 0.4

Notes.
[a] All lines are observed with *Herschel*/HIFI except CO 3–2 which is observed with JCMT/HARP-B.
[b] Frequencies are from the Jet Propulsion Laboratory molecular database (Pickett et al. 1998).

CO 10–9, ^{13}CO 10–9, and [C II]158 μm lines have a different profile than H_2O, with a single peak near systemic velocity (at $V_{LSR} = +6.5$ km s^{-1} in CO and +5.5 km s^{-1} in [C II]), and a pronounced blue wing extending down to 0 and −5 km s^{-1}, respectively (i.e., 6 and 11 km s^{-1} away from systemic). The bulk of CO and [C II] emission close to systemic velocity likely originates in the envelope, as suggested by the ^{13}CO 2–1 channel maps by Testi et al. (2002) which indicate emission extended over ≃10″ at velocities $|V - V_{sys}| < 1.5$ km s^{-1}. The observed blue wing, instead, may originate in a slow outflow, perhaps linked to envelope dispersal motions, as proposed by Kitamura et al. (1996). For the [C II]158 μm line, an origin in an extended structure is further confirmed by the fact that the flux in the HIFI beam of ∼11″ is ∼4 times lower than the total co-added flux in the *Herschel*/PACS observations (47″×47″; Podio et al. 2012).

On the other hand, several arguments suggest that the H_2O emission is compact and is likely dominated by emission from the outer region of the protoplanetary disk of DG Tau and not from the envelope/outflow.

1. The H_2O line profiles are different from those of CO and [C II] observed with single-dish telescopes. They are much more symmetric about the systemic velocity and do not show the extended blue wing seen in these other tracers.
2. The peaks of the H_2O line profiles coincide with the two narrow velocity ranges ($|V - V_{sys}| = 1.5$–2.5 km s^{-1}) where ^{13}CO 2–1 interferometric maps show compact emission with a velocity gradient perpendicular to the jet axis, consistent with disk rotation (Testi et al. 2002). The ^{13}CO 2–1 line profile obtained by integrating the interferometric maps by Testi et al. (2002) over a 2″ beam, i.e., by cutting out any extended component, is similar to the H_2O line profiles, with peaks at the same velocities. In contrast, the CO 3–2 profile, obtained with the JCMT collecting all the emission in the 14″ beam, does not peak at the same velocity as the H_2O and ^{13}CO compact component. This is particularly clear in the blue part of the profile.
3. Assuming Keplerian rotation, and an inclination of $i \simeq 38°$ from the line of sight (Eislöffel & Mundt 1998), the peak separation of the H_2O lines ($\Delta V_{sep} \sim$ 3–3.5 km s^{-1}) indicates an outer disk radius $R_{out}(H_2O) \sim$ 77–105($M_\star/0.7\ M_\odot$) AU. For a stellar mass of ∼0.7 $M_\odot$, as assumed in Testi et al. (2002), the inferred $R_{out}(H_2O)$ is in agreement with the disk outer radius, ∼72–89 AU, estimated from sub-arcsecond dust continuum maps at 1.3 and 2.8 mm with CARMA (Isella et al. 2010). The maximum velocities covered by the line profiles, instead, set an

[12] *Herschel* is an ESA space observatory with science instruments provided by European-led Principal Investigator consortia and with important participation from NASA.
[13] HIPE is a joint development by the *Herschel* Science Ground Segment Consortium, consisting of ESA; the NASA *Herschel* Science Center; and the HIFI, PACS, and SPIRE consortia.
[14] http://www.iram.fr/IRAMFR/GILDAS

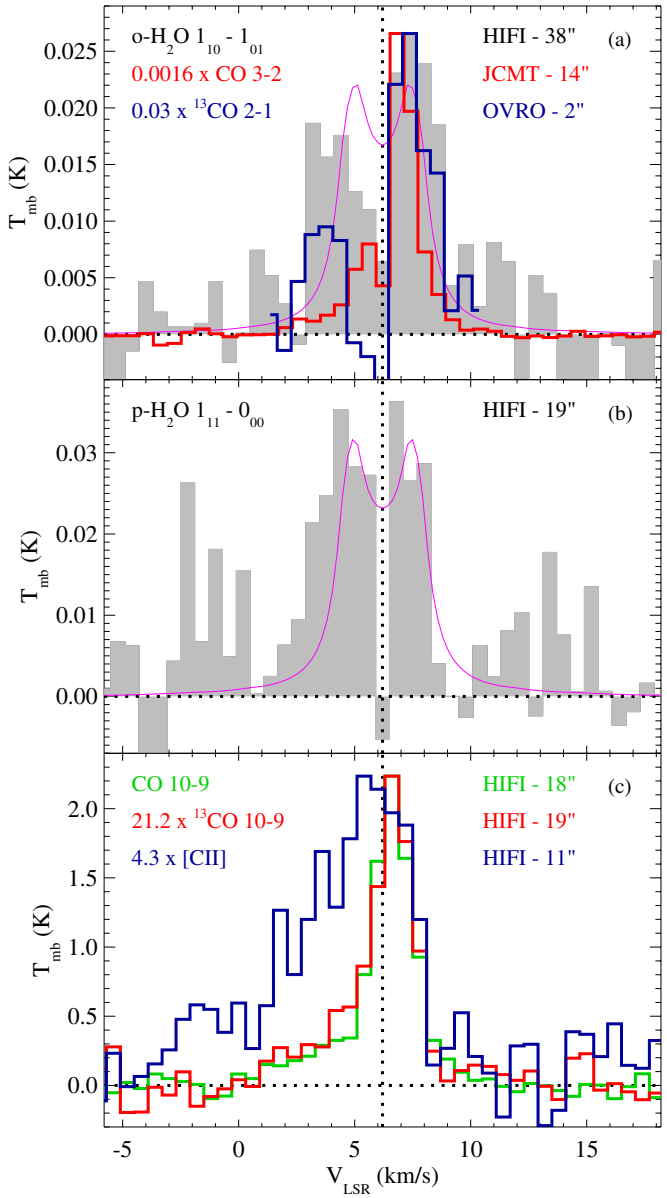

Figure 1. HIFI spectra of (a) o-H_2O 1_{10}-1_{01} (gray histogram); (b) p-H_2O 1_{11}-0_{00} (gray histogram); (c) CO 10–9, ^{13}CO 10–9, and [C II] $^2P_{3/2}$-$^2P_{1/2}$ (green, red, and blue histograms, respectively). In panel (a) JCMT CO 3–2 (red histogram) and ^{13}CO 2–1 profiles obtained integrating interferometric maps by Testi et al. (2002) on a 2″ beam (blue histogram) are also shown. The vertical dotted line indicates the systemic velocity (V_{LSR} = +6.2 km s^{-1}). The H_2O line profiles predicted by the "low dust opacity" ProDiMo disk model are overplotted (magenta lines). The o-H_2O line flux is underpredicted by the model by a factor of ∼2.2; hence, the line profile is multiplied by this factor to help the comparison with observations.

(A color version of this figure is available in the online journal.)

upper limit to the inner radius of the line emitting region $R_{in}(H_2O) \leqslant 19$ AU, since more extended line wings could be hidden in the noise.

4. The H_2O line profiles are reproduced by an optically thick, vertically isothermal Keplerian disk with $T_{ex} \propto r^{-0.5}$ viewed at 38° with an excitation temperature at R_{out} of 70 and 32 K for the ortho and para lines, respectively (Beckwith & Sargent 1993; Cabrit et al. 2006).

Given the evidence listed above, the fundamental water lines, even when observed with a 38″–19″ beam, appear to be dominated by compact emission. Although we cannot exclude contamination from the outflow, which could explain the larger FWHM and the asymmetry of the o-H_2O 557 GHz, the detected double-peaked H_2O lines prove to be a good tracer of the outer protoplanetary disk of DG Tau, with less confusion from envelope/outflow than in ^{13}CO.

DG Tau shows emission also in high-excitation H_2O lines observed with PACS (Podio et al. 2012). With $E_{up} \sim$ 200–1070 K these are thought to originate in an intermediate disk region between a few and a few tens of astronomical units from the star (e.g., Riviere-Marichalar et al. 2012). The exception is the low-excitation H_2O 179.5 μm line ($E_{up} \sim$ 114 K) which, according to previous disk modeling, is predicted to form in the outer disk like the 557 and 1113 GHz lines (Kamp et al. 2013). The observed H_2O 179.5 μm/557 GHz line ratio is $R1_{obs} = 22 \pm 6$, consistent with LTE optically thick emission in the Rayleigh–Jeans limit, i.e., for temperatures larger than a few hundred Kelvin ($R_{LTE-thick} \sim 27$). On the other hand, the line ratio between the para- and the ortho-fundamental lines ($R2_{obs} = 2.5 \pm 0.3$) is around three times lower than $R_{LTE-thick} \sim 8$. This can be explained if the lines are excited in a region where the gas density is lower than the lines' critical density (∼2×10^7 and ∼2×10^8 at 50 K for the 557 and 1113 GHz lines) and/or where the temperature is below their upper level energies. Also, the observed line ratio could be affected by emission from the envelope/outflow.

4. MODELING H_2O IN THE DISK OF DG Tau

Detailed disk modeling is required to test the disk hypothesis and to derive an estimate of the water mass. The latter cannot be inferred from observations since the lines are likely optically thick. We include in our analysis the fluxes and upper limits obtained for the water lines falling between 63.3 and 180.5 μm observed with PACS as part of the *Herschel* Key Project GASPS (PI: B. Dent; Podio et al. 2012). The two detected o-H_2O lines at 78.7 and 179.5 μm are spectrally and spatially unresolved, thus their origin is unclear. In Podio et al. (2012) a shock origin was favored based on the large line fluxes, which are difficult to reproduce with disk models for typical TTS parameters. However, since the profiles of the ground-state water lines are consistent with a disk origin, we test the predictions of a dedicated model for DG Tau by comparing them with observed H_2O line fluxes and profiles.

We use a parameterized disk model calculated with the thermo-chemical disk modeling code ProDiMo (Woitke et al. 2009; Kamp et al. 2010). We adopt the stellar spectral type K7 ($T_{eff} \simeq$ 4000 K) and veiling-corrected stellar radius of 1.8 $R_\odot$ (Fischer et al. 2011). The resulting stellar luminosity ≃1 $L_\odot$ yields a stellar mass $M_\star \simeq 0.7\ M_\odot$ and an age of 2.5×10^6 yr using the evolutionary tracks of Siess et al. (2000). To reproduce the *IUE* UV/optical spectrum (Gullbring et al. 2000), we set the UV excess fraction $f_{UV} = L(910\text{–}2500\,\text{Å})/L_* = 0.2$ and adopt a power-law slope $L_\lambda \approx \lambda^{-0.3}$. We also account for the effect of X-ray radiation from the stellar corona ($L_X = 10^{30}$ erg s^{-1}; Güdel et al. 2007) following Aresu et al. (2011) and Meijerink et al. (2012). The disk inner and outer radius are set to $R_{in} = 0.16$ AU (Akeson et al. 2005) and $R_{out} = 100$ AU, in agreement with $R_{out}(H_2O)$ inferred from the observed H_2O profiles. We assume the dust size distribution and disk dust mass from the "low dust opacity model"—a 50/50 mixture of astronomical silicates (Draine & Lee 1984) and amorphous carbon (Zubko et al. 1996)—used by Isella et al. (2010) to reproduce the observed 1.3 and 2.8 mm emission ($n(a) \approx a^{-q}$

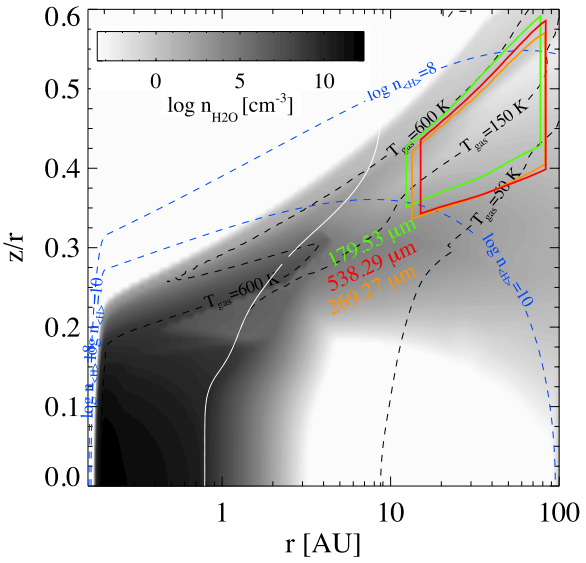

Figure 2. Disk region from which 50% of the o-H_2O179.5 μm (in green), o-H_2O538.3 μm (or 557 GHz, in red), and p-H_2O269 μm (or 1113 GHz, in orange) line emission arises according to the "low dust opacity" disk model. The gray color indicates the water density, n_{H_2O} (cm^{-3}), the dotted black and blue curves indicate the gas temperature and density, and the white solid curve indicates the snow line (i.e., T_{dust} = 150 K).

(A color version of this figure is available in the online journal.)

with $q = 3.5$, where a is the dust grain radius; the minimum/maximum grain sizes are $a_{min} = 0.005$ μm and $a_{max} = 5$ cm). Using the standard dust-to-gas ratio of 0.01, the gas mass is set to 0.1 $M_\odot$. The disk is thought to be perpendicular to the jet, thus $i = 38°$(Eislöffel & Mundt 1998). We assume a parameterized disk shape with a surface density $\Sigma \approx r^{-1}$ and a scale height $H = 0.008\,\mathrm{AU}(r/0.16\,\mathrm{AU})^{1.2}$. No dust settling is invoked, i.e., dust and gas are well mixed throughout this young disk. The polycyclic aromatic hydrocarbon (PAH) fraction is 0.01 with respect to the interstellar medium (ISM) abundance of $10^{-6.52}$ PAH particles/H-nucleus. All parameters adopted for the model are summarized in Table 2.

The line profiles and fluxes are obtained by first solving the statistical equilibrium with two-dimensional (2D) escape probability to obtain the level populations, and then using 2D radiative transfer (collision rates as listed in Table 3 of Kamp et al. 2013). The region from which 50% of the H_2O line emission arises, instead, is obtained using vertical escape probability and without accounting for disk inclination. Figure 2 indicates that the H_2O179.5 μm line observed with PACS originates in the same region as the fundamental water lines at 557 and 1113 GHz observed with HIFI, i.e., in an upper disk layer ($z/r \sim 0.35$–0.6) located at ~10–90 AU distance from the star. In this region the gas temperature is ~50–600 K and water is formed mainly through gas-phase reactions and partially dissociated by UV photons and collisions with C^+ and H^+. Including self-shielding for all photodissociating species produces at most 20% lower fluxes. The gas density is 10^8–10^{10} cm^{-3}; thus, as suggested by the observed H_2O179.5 μm/557 GHz line ratio, these lines are close to LTE and optically thick ($\tau \sim 10^3$–10^4). The ortho-to-para ratio (OPR) is calculated from the gas temperature at thermal equilibrium and is 1.5–3 in the line emitting region. However, since the H_2O lines are optically thick, the model results are not dependent on the OPR.

Table 2
"Low Dust Opacity" Disk Model: Star and Disk Parameters

Effective temperature	T_{eff} (K)	4000
Stellar mass	M_* ($M_\odot$)	0.7
Stellar luminosity	L_* ($L_\odot$)	1
UV excess	f_{UV}	0.2
UV power-law index	p_{UV}	−0.3
X-ray luminosity	L_X (erg s^{-1})	10^{30}
Disk inner radius	R_{in} (AU)	0.16
Disk outer radius	R_{out} (AU)	100
Disk dust mass	M_{dust} ($M_\odot$)	1×10^{-3}
Dust-to-gas ratio	dust to gas	0.01
Solid material mass density	ρ_{dust} (g cm^{-3})	3.5
Minimum grain size	a_{min} (μm)	0.005
Maximum grain size	a_{max} (cm)	5
Dust size distribution index	q	3.5
Disk inclination	i (°)	38
Surface density $\Sigma \approx r^{-\epsilon}$	ϵ	−1
Scale height at R_{in}	H_0 (AU)	0.008
Disk flaring index $H(r) = H_0(\frac{r}{R_{in}})^\beta$	β	1.2
Fraction of PAHs w.r.t. ISM	f_{PAH}	0.01

Table 3
Observed and Disk-model-predicted H_2O Fluxes

Line	λ (μm)	E_{up} (K)	$F_{obs} \pm \Delta F$ (W m^{-2})	F_{mod} (W m^{-2})
PACS observations				
o-H_2O	63.3	1070	$\leqslant 4 \times 10^{-17}$	1.9×10^{-17}
o-H_2O	71.9	843	$\leqslant 1 \times 10^{-17}$	1.7×10^{-17}
o-H_2O	78.7	432	$1.9 \pm 1.4 \times 10^{-17}$	2.1×10^{-17}
o-H_2O	179.5	114	$1.5 \pm 0.3 \times 10^{-17}$	7.7×10^{-18}
o-H_2O	180.5	194	$\leqslant 1 \times 10^{-17}$	3.2×10^{-18}
p-H_2O	78.9	781	$\leqslant 1 \times 10^{-17}$	9.7×10^{-18}
p-H_2O	89.9	297	$\leqslant 1 \times 10^{-17}$	1.4×10^{-17}
p-H_2O	144.5	396	$\leqslant 1 \times 10^{-17}$	2.7×10^{-18}
p-H_2O	158.3	410	$\leqslant 1 \times 10^{-17}$	3.9×10^{-19}
HIFI observations				
o-H_2O	538.3	61	$6.7 \pm 0.7 \times 10^{-19}$	3.1×10^{-19}
p-H_2O	269.3	53	$1.7 \pm 0.2 \times 10^{-18}$	1.9×10^{-18}

As shown in Figure 1 the model reproduces the p-H_2O line flux and profile, and the ratio o-H_2O 179.5 μm/557 GHz is $R1_{mod} \simeq 25$, in agreement with the observed value. On the other hand, the observed ortho lines at 179.5 μm and 557 GHz are underpredicted by a factor of ~2. As a consequence, the observed p-H_2O 1113/o-H_2O 557 line ratio is overpredicted by a factor of 2.4 ($R2_{mod} = 6.1$). Kamp et al. (2013) discuss in detail the uncertainties when modeling water emission in disks. They show that the assumed surface chemistry, adsorption energy and photodesorption yields, and metal abundances can affect water line fluxes by a factor of a few. In particular, the low-excitation water lines are very sensitive to the adopted radiative transfer method and to the uncertainties in the collision rates. Moreover, the disk model is not accounting for the X-ray emission by the jet (Güdel et al. 2008) which illuminates the disk surface from above. This may boost water formation through H_3O^+ recombination ($H_3O^+ + e^- \rightarrow H_2O + H$; Meijerink et al. 2012). In general, the model can reproduce all the H_2O lines observed with PACS and HIFI within a factor of two (see Table 3). The emission in the CO and [C II] lines is predicted to be a factor of 3–9 lower than observed, suggesting that the bulk of the

emission originates from the envelope/outflow as indicated by the observed profiles.

The disk model indicates that the disk contains ~0.4 $M_\oplus$ of water vapor, and two orders of magnitude larger mass in ice: $M(H_2O\#) \sim 100\ M_\oplus$. To understand the reliability of the estimated water mass in the disk, we calculate a second model assuming the dust size distribution and disk dust mass from the "high dust opacity model" by Isella et al. (2010). This implies around an order of magnitude lower dust mass in the disk and consequently around an order of magnitude lower gas mass, and water vapor and ice mass ($M_{gas} = 0.015\ M_\odot$, $M(H_2O) \sim 0.06\ M_\oplus$, $M(H_2O\#) \sim 7\ M_\oplus$). We find that this model can reproduce equally well the observed H_2O line fluxes, because the "high dust opacity model" implies lower opacity at UV wavelengths and thus a deeper UV penetration in the outer disk regions. Hence, the dust size distribution is crucial to constrain the disk mass and water reservoir, leading to an uncertainty of one order of magnitude. The total water reservoir, $M(H_2O)_{gas+ice} \sim 7$–$100\ M_\oplus$, is a factor of a few up to two orders of magnitude larger than for TW Hya (Hogerheijde et al. 2011).

5. CONCLUSIONS

The present detection of the o-H_2O and p-H_2O lines at 557 and 1113 GHz in the TTS DG Tau is crucial for several reasons: (1) so far, emission in the fundamental water lines has been observed only in one TTS, TW Hya; (2) we detect for the first time a double-peaked profile in the H_2O lines, which is strong kinematic evidence for an origin in the outer disk (from ~10–90 AU); (3) water is a unique tracer of the protoplanetary disk of DG Tau because it is less contaminated by envelope/outflow emission than CO lines; (4) once corrected for distance, the H_2O lines are ~19–26 times brighter than in TW Hya. According to our models, the reason is the 10 times higher UV flux of DG Tau, which heats the outer disk surface layer up to temperatures of ~600 K (only ~30 K in the case of TW Hya). In addition, the disk around DG Tau is more massive and compact, leading to higher volume densities in the surface layers, which makes the warm neutral chemistry even more efficient; (5) the adopted models suggest a disk mass of 0.015–0.1 $M_\odot$, depending on the assumed dust size distribution, and a water reservoir (gas+ice) of 7–100 $M_\oplus$, i.e., at least a factor of a few larger than estimated for TW Hya (Hogerheijde et al. 2011).

While the inferred disk mass is consistent with the minimum mass of the solar nebula needed to form our solar system, the detection of water vapor in the outer region of the disk, where comets are believed to form, and the estimated water mass of a few $\sim 10^4$–10^5 Earth oceans, supports the scenario of impact delivery of water on terrestrial planets by means of icy bodies.

L.P. and C.P. acknowledge funding from the European 7th Framework Program (FP7; contracts PIEF-GA-2009-253896 and PERG06-GA-2009-256513), and from Agence Nationale pour la Recherche (ANR; contract ANR-2010-JCJC-0504-01). We also acknowledge funding from FP7-2011 (contract 284405), and the Service Commun de Calcul Intensif de l'IPAG for computations (contracts ANR-07-BLAN-0221, ANR-2010-JCJC-0504-01, and ANR-2010-JCJC-0501-01).

REFERENCES

Akeson, R. L., Boden, A. F., Monnier, J. D., et al. 2005, ApJ, 635, 1173
Aresu, G., Kamp, I., Meijerink, R., et al. 2011, A&A, 526, A163
Beckwith, S. V. W., & Sargent, A. I. 1993, ApJ, 402, 280
Bergin, E. A., Hogerheijde, M. R., Brinch, C., et al. 2010, A&A, 521, L33
Cabrit, S., Pety, J., Pesenti, N., & Dougados, C. 2006, A&A, 452, 897
Carr, J. S., & Najita, J. R. 2008, Sci, 319, 1504
Ceccarelli, C., Dominik, C., Caux, E., Lefloch, B., & Caselli, P. 2005, ApJL, 631, L81
de Graauw, T., Helmich, F. P., Phillips, T. G., et al. 2010, A&A, 518, L6
Dominik, C., Ceccarelli, C., Hollenbach, D., & Kaufman, M. 2005, ApJL, 635, L85
Dougados, C., Cabrit, S., Lavalley, C., & Ménard, F. 2000, A&A, 357, L61
Draine, B. T., & Lee, H. M. 1984, ApJ, 285, 89
Eislöffel, J., & Mundt, R. 1998, AJ, 115, 1554
Fischer, W., Edwards, S., Hillenbrand, L., & Kwan, J. 2011, ApJ, 730, 73
Güdel, M., Skinner, S. L., Audard, M., Briggs, K. R., & Cabrit, S. 2008, A&A, 478, 797
Güdel, M., Telleschi, A., Audard, M., et al. 2007, A&A, 468, 515
Gullbring, E., Calvet, N., Muzerolle, J., & Hartmann, L. 2000, ApJ, 544, 927
Hartigan, P., Edwards, S., & Ghandour, L. 1995, ApJ, 452, 736
Hogerheijde, M. R., Bergin, E. A., Brinch, C., et al. 2011, Sci, 334, 338
Isella, A., Natta, A., Wilner, D., Carpenter, J. M., & Testi, L. 2010, ApJ, 725, 1735
Kamp, I., Thi, W.-F., Meeus, G., et al. 2013, A&A, submitted
Kamp, I., Tilling, I., Woitke, P., Thi, W.-F., & Hogerheijde, M. 2010, A&A, 510, A18
Kitamura, Y., Kawabe, R., & Saito, M. 1996, ApJ, 457, 277
Kristensen, L. E., van Dishoeck, E. F., Bergin, E. A., et al. 2012, A&A, 542, A8
Lecar, M., Podolak, M., Sasselov, D., & Chiang, E. 2006, ApJ, 640, 1115
Matsui, T., & Abe, Y. 1986, Natur, 322, 526
Meijerink, R., Aresu, G., Kamp, I., et al. 2012, A&A, 547, A68
Pickett, H. M., Poynter, R. L., Cohen, E. A., et al. 1998, JQSRT, 60, 883
Pilbratt, G. L., Riedinger, J. R., Passvogel, T., et al. 2010, A&A, 518, L1
Podio, L., Kamp, I., Flower, D., et al. 2012, A&A, 545, A44
Pontoppidan, K. M., Salyk, C., Blake, G. A., & Käufl, H. U. 2010a, ApJL, 722, L173
Pontoppidan, K. M., Salyk, C., Blake, G. A., et al. 2010b, ApJ, 720, 887
Riviere-Marichalar, P., Ménard, F., Thi, W. F., et al. 2012, A&A, 538, L3
Roelfsema, P. R., Helmich, F. P., Teyssier, D., et al. 2012, A&A, 537, A17
Salyk, C., Pontoppidan, K. M., Blake, G. A., et al. 2008, ApJL, 676, L49
Schuster, K. F., Harris, A. I., Anderson, N., & Russell, A. P. G. 1993, ApJL, 412, L67
Siess, L., Dufour, E., & Forestini, M. 2000, A&A, 358, 593
Testi, L., Bacciotti, F., Sargent, A. I., Ray, T. P., & Eislöffel, J. 2002, A&A, 394, L31
Woitke, P., Kamp, I., & Thi, W.-F. 2009, A&A, 501, 383
Zubko, V. G., Mennella, V., Colangeli, L., & Bussoletti, E. 1996, MNRAS, 282, 1321